https://doi.org/10.5194/egusphere-2025-856
Preprint. Discussion started: 20 March 2025

Deciphering Dust Provenance and Transport Pathways Across Northern China's Source-Sink Systems

Lanying Han[1], Zhengyu Zhang[1], Aimin Liang[1], Junfeng Lu[2], Zhibao Dong[1], Zhengcai Zhang*[1,2],

[1] Key Laboratory of Qian Xuesen Deserticulture of Shaanxi Higher Education Institute, School of Geography and Tourism, Shaanxi Normal University, Xi'an 710119, China

[2] Northwest Institute of Eco-environment and Resources, Chinese Academy of Sciences, Lanzhou 730000, China

* Corresponding author: School of Geography and Tourism, Shaanxi Normal University, Xi'an 710119, China.

E-mail address: zhangzhengcai@snnu.edu.cn

Abstract: Northern China's arid lands constitute one of Earth's most active aeolian ecosystems, yet persistent uncertainties remain regarding the precise source apportionment of dust emissions impacting downstream regions. By applying advanced geochemical fingerprinting techniques to modern airborne dust samples collected across major potential source areas (Taklimakan, Gurbantunggut, Hexi Corridor, Heihe River Basin, Gurbantunggut, Alxa Plateau, and Qaidam Basin Desert), we systematically quantified dust provenance through coupled rare earth element signatures and trace element ratios. Our multivariate analysis reveals three critical findings: (1) The Taklimakan and Gurbantunggut deserts dominate as primary sources than Gobi Desert (Alxa Plateau, Hexi Corridor and Heihe Basin) and the Qaidam Basin Desert; (2) Despite the Taklimakan and Gurbantunggut Desert's upwind position relative to the CLP, the intervening Alxa Plateau (>1,500 m asl) acts as a topographic filter of dust destined for the Lanzhou and Mu Us regions while facilitating multi-phase recycling through localized deposition and remobilization; (3) Provenance shifts exhibit strong spatial dependency, with Lanzhou's dust load dominated by Gurbantunggut sources (26.1%), then Taklimakan (18.3%); but Mu Us dust dominated by Alxa (27.5%), then Taklimakan (21.6%). These findings redefine our understanding of East Asian dust dynamics by demonstrating how elevation barriers and sedimentary recycling jointly modulate source-sink relationships over millennial scales.

Keywords: Aeolian dust provenance; Geochemical fingerprinting; Topographic barrier; Sediment recycling; Chinese Loess Plateau; HYSPLIT trajectory analysis

https://doi.org/10.5194/egusphere-2025-856
Preprint. Discussion started: 20 March 2025

1. Introduction

Atmospheric mineral dust serves as a critical agent in Earth system dynamics, modulating radiative forcing (Lambert et al., 2008; Kok et al., 2023), decreased air quality (Prospero, 1999; Tanaka and Chiba, 2006; Shao et al., 2010; Chen et al., 2020), perturbing biogeochemical cycles (Jickells et al., 2005), and posing significant public health risks through particulate matter exposure (Prospero, 1999; Goudie, 2014). Asia dominates the global dust budget, contributing up to 32% of total emissions (Tanaka & Chiba, 2006), yet substantial uncertainties persist regarding the precise quantification of Asian dust fluxes (range: 25–400 Mt yr^{-1}; Xuan et al., 2000; Laurent et al., 2006) and the spatial attribution of source-to-sink pathways.

While land surface parameters—including grain size distribution, vegetation cover, and soil crust integrity—exert first-order controls on dust emission thresholds (Marticorena et al., 1997; Webb et al., 2014), emerging evidence highlights the underappreciated role of regional geomorphology in modulating dust transport efficiency (Batt and Peabody, 1999; Gillette et al., 2004; Zhang et al., 2008;). In northern China, the juxtaposition of high-elevation barriers (Alxa Plateau: 3340 m; Qilian Mountains: 5808 m) and arid basins creates a topographic "filter" system that redirects, deposits, and remobilizes dust along transport corridors (Sun et al., 2018). Recent isotopic studies reveal that >60% of dust deposited on the Chinese Loess Plateau (CLP) undergoes multistage recycling through these transitional zones (Zhang et al., 2025), yet the mechanisms governing source-sink connectivity remain enigmatic. A critical knowledge gap persists: how do elevation barriers and sedimentary reworking alter provenance signatures across spatiotemporal scales?

At present, four main dust sources to the CLP have been previously proposed: the Hexi Corridor and adjacent regions (Sun, 2002; Sun et al., 2018), the northeastern Tibetan Plateau (i.e., the Qaidam Basin Desert or via the Yellow River and Yinchuan-Hetao Graben alluvial platform) (Stevens et al., 2010; Kapp et al., 2011; Nie et al., 2015; Bird et al., 2015), the Taklimakan Desert (Liu et al., 1994), and multiple sources distributed throughout the region (Chen et al., 2007; Maher et al., 2009). These disputes

https://doi.org/10.5194/egusphere-2025-856
Preprint. Discussion started: 20 March 2025

over the dominant sources have arisen, in part, from different definitions of a dust source region (Sun et al., 2020), different sample collection methods (e.g., surface samples, meteorological observations), and different selection of the optimal geochemical fingerprints (Liu et al., 1994; Ding et al., 2001; Chen et al., 2007).

Analysis of the geochemical or mineralogical characteristics of surface sediment samples has been the most popular approach to identifying the provenance (Zhang et al., 2025). However, surface samples may have experienced multiple episodes of mixing and recycling in the source regions and during transport (Ding et al., 2001; Jahn et al., 2001), complicating source assignment. Two main groups of factors affect these processes. First, dust depositional regions that have similar geomorphology in their original areas appear to have similar dust sources. For example, the Qilian Mountains can provide dust for both the Qaidam Basin Desert, Heihe River Basin and the Hexi Corridor Desert, whereas the Heihe River Basin (downwind of the Alxa Plateau) appears to be a main dust source for all of northern China (Zhang et al., 2022a). Second, different dust depocentres that lie along the same wind transport pathways appear to have similar dust sources when wind velocity decreased at the leeward of mountains or basins (Tan et al., 2021). Deposition occurs when wind speed decreases below the dust emission threshold wind velocity (Zhang et al., 2016). Therefore, using surface samples could lead to ambiguities for the mixing and recycling in the dust source regions, and it is necessary to sample airborne dust to better identify dust provenance.

Traditional provenance methods relying on surface sediment geochemistry face inherent limitations. Bulk geochemical analyses (Gallet et al., 2001; Jahn et al., 2001), detrital zircon U-Pb dating (Stevens et al., 2010; Pullen et al., 2011; Nie et al., 2014, 2015; Rittner et al., 2016; Sun et al., 2018; Fenn et al., 2018; Bohm et al., 2022), and heavy mineral assemblages (Rittner et al., 2016) often conflate primary emissions with recycled material, as demonstrated by the discordant REE signatures between Hexi Corridor surface sediments and vertically transported dust (Zhang et al., 2025). This discrepancy underscores the necessity of direct airborne sampling to decouple source-specific fingerprints from transport-mediated mixing.

Methodological advancements further challenge conventional approaches. While early studies relied on bivariate element ratios (Jahn et al., 2001) or qualitative similarity indices (Hu and Yang, 2016), modern provenance analysis demands multivariate frameworks capable of resolving overlapping geochemical signals. Herein, we integrate multi-dimensional scaling (MDS) and Bayesian linear unmixing models—tools proven effective in sedimentology (Collins et al., 2010; Vermeesch, 2013; Zhang et al., 2020) but underutilized in dust studies—to quantify source contributions while accounting for topographic forcing.

This study addresses three unresolved questions: Which geochemical fingerprints (REE vs. trace elements) most robustly discriminate northern China's dust sources? How do the Alxa Plateau and Qilian Mountains regulate dust transit from the Gurbantunggut Desert to the CLP? What proportion of CLP dust derives from primary sources versus recycled deposits? By analyzing 214 modern airborne dust samples across seven key regions (Taklimakan Desert to Tengger Desert), we establish a novel provenance framework that reconciles geochemical tracers with topographic dynamics. Our findings not only redefine East Asian dust source hierarchies but also provide a mechanistic template for predicting dust response to future climate-driven landscape changes.

2. Study region and methods

2.1 Study region

The study area encompasses major dust source regions across northern China (Fig. 1), governed by the Mongolia-Siberia High-Pressure System. The dust storm frequency is higher (more than 50 days per year) during this period and is related to the East Asian Winter Monsoon (Wyrwoll et al., 2016). Annual precipitation increases from 40 mm (Ejina, hyper-arid) to 438 mm (Yulin, semi-arid) along the NW-SE transect. Drift Potential (*DP*) decreases from >400 VU at Mazong to 70 VU at Yulin, with Resultant Drift Direction (*RDD*) consistently NW-SE (Zhang et al., 2016; Liu and Yang, 2018; Table S2). Gravel cover exceeds 55% across Gobi deserts, with widespread physical soil crusts (Zhang et al., 2016).

https://doi.org/10.5194/egusphere-2025-856
Preprint. Discussion started: 20 March 2025

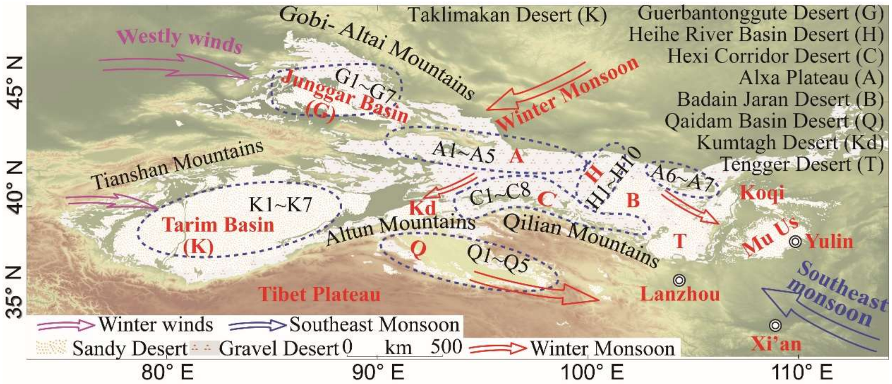

Figure 1. Locations of the gobi (gravel) and sandy deserts in northern China, and the associated wind systems.

2.2 Methods

Here we defined Taklimakan Desert (K1~K7) and Gurbantunggut Desert (G1~G7) are upwind regions for these two regions were primary emission areas. The Qaidam Basin Desert (Q1~Q5), Alxa Plateau (A1~A5), Hexi Corridor Desert (C1~C8), Heihe River Basin (H1~H10), and Tengger Deserts (T1~T2) are middle regions for deposition-remobilization belt. Lanzhou (L), Mu Us Desert (M) as downwind regions for terminal sinks (Fig. 1, Table 1).

Table 1 Sample name, sample size (*n*), surface properties, sample height, and locations of the sample sites. Figure 1 shows the locations of the samples (Location showed in Fig. S1). Sample location names: A, Alxa Plateau; C, Hexi Corridor Desert; G, Gurbantunggut Desert; H, Heihe River Basin; K, Taklimakan Desert; L, Lanzhou; M, Mu Us Desert; Q, Qaidam Basin Desert; T, Tengger Desert.

Sample	*n*	Surface types	Height	Crust
A1 to A5	5	Flat gravel Gobi	Surface	√
C1 to C3	3	Flat gravel Gobi	Surface	√
C4 to C8	6	Flat gravel Gobi	2 m	√
G1 to G7	7	Dry lacustrine dunes (<20 m)	Surface	√
H1 to H4	4	Alluvial fan Gobi	Surface	√
H5 to H10	6	Alluvial fan Gobi	2 m	√
K1 to K7	7	Mobile dunes	2 m	×
L	1	Urban settled dust	10 m	×
M	1	Fixed dunes	10 m	√
Q1 to Q3	3	Flat gravel Gobi	Surface	√
Q4	1	Dry lakebed	2 m	√
Q5	1	Flat gravel Gobi	2 m	√

https://doi.org/10.5194/egusphere-2025-856
Preprint. Discussion started: 20 March 2025

T1-T2	1	Mobile dunes	10 m	×

Transported dust materials were collected by modified the Big Spring Number Eight traps (Fryrear, 1986) at a height of 2 m in the dust source regions at a height of 10 m in southeastern Tengger Desert and Mu Us Desert (Fig. 1, Table 1), and on the sediment surface in one depositional region (Lanzhou, Fig. 1). In total, we collected 47 field samples (22 land surface samples and 25 transported dust samples, Table 1). These samples were collected at the end of Spring 2019. Surface samples were collected from a 40 cm×40 cm quadrats (to a depth of 1 cm) at each site. Each sample weighed 0.5 to 1.0 kg. Further information of the Big Spring Number Eight traps is provided by Zhang et al. (2016).

Samples were dry-sieved at 63 µm to isolate long-range transportable particles. REE and trace element contents were measured using an inductively coupled plasma emission mass spectrometer (PlasmaQuant-MS Elite, Analytikjena, Jena, Germany) at the Institute of Geochemistry, Chinese Academy Sciences, Guiyang. Rh was used as the internal standard. The samples were digested for 12 h in a 1:1 v/v mixture of 0.5 mL HNO_3 and 1 mL HF at 190°C in screw-top PTFE-lined stainless steel bombs following the four-step procedure described by Liang et al. (2000). The analytical uncertainties (coefficient of variation) were less than ±5% for REE (La, Ce, Pr, Nd, Sm, Eu, Gd, Tb, Dy, Ho, Er, Tm, Yb, and Lu) and less than ±10% for trace elements (Li, Be, Sc, V, Cr, Co, Ni, Cu, Zn, Ga, Ge, As, Rb, Sr, Y, Zr, Nb, Mo, Ag, Cd, In, Sn, Sb, Cs, Ba). Table S3 summarizes the contents for all elements.

2.3 Data analysis

2.3.1 Fingerprint Selection

Zhang et al., (2020) indicated that MDS and PCA can be well identify Aeolian sediment provenance in the northern China desert regions. Therefore, we used MDS and principal-components analysis (PCA) to identify the best elements to create composite fingerprints for each sample (Vermeesch, 2013; Rittner et al., 2016; Zhang et al., 2020).

2.3.2 Spatial Clustering

Non-metric Multidimensional Scaling (MDS) with Kolmogorov-Smirnov statistics (*KS*), using Canberra distance matrix (Stress) to identify affinities and differences among samples based on the statistical dissimilarity of their compositional signatures

https://doi.org/10.5194/egusphere-2025-856
Preprint. Discussion started: 20 March 2025

(Vermeesch, 2013; Vermeesch et al., 2016), and has been widely used (Stevens et al., 2013; Vermeesch, 2013; Rittner et al., 2016; Zhang et al., 2020). We used the final stress value to evaluate the goodness of fit of the MDS configuration according to Kruskal's (1964) classification and used version 3.5.1 of the R software for this analysis (Vermeesch, 2013). We used the Kruskal-Wallis test, multivariate discriminant function analysis, and a Euclidean distance matrix to improve the model's accuracy (Collins et al., 2010; Gaspar et al., 2019).

2.3.3 Provenance budget

We calculated the relative contributions of different sources for each sample using a Bayesian mixing models for the advantages of considering prior information, and uncertainty (Luo et al., 2022). The model well explained the spatial variability of fingerprint attributes, the uncertainty of residuals between fingerprint attributes, and model error (Cooper et al., 2015). Root mean square error (*RMSE*) and mean absolute error (*MAE*) were used to evaluate the accuracy of the model. We used all samples and the trace and REE element ratios identified in section 2.3.1 in the calculation model.

3. Results

3.1 Trace element fingerprinting

The PCA of trace elements revealed three dominant components explaining 82.5% cumulative variance (PC1=47.7%, PC2=26.2%, PC3=8.7%; Table S4). Six elements—Sc, Y, Zr, Nb, Hf, and Ta—emerged as optimal discriminators (ANOVA, $P<0.05$), forming distinct geochemical clusters across source regions (Fig. 2). Kruskal-Wallis tests identified three elements with significant spatial differentiation ($P<0.05$) (Fig. 3). Ba was 624.89±91.20 μg/g for the Alxa Plateau and Hexi Corridor (672.50±374.64 μg/g) tripled those of Taklimakan Desert (264.89±44.66 μg/g; ***$P<0.001$). Nb progressive enrichment occurred along transport pathways: Taklimakan (7.64±1.95 μg/g) → Heihe Basin (13.89±4.37 μg/g; **$P<0.01$). Y in the western sources (Gurbantunggut: 28.58±7.31 μg/g) showed 43% lower concentrations than eastern sinks (CLP: 50.12±9.45 μg/g; *$P<0.05$). These patterns suggest strong hydrodynamic fractionation during transport, with finer-grained Nb-Y rich particulates preferentially

https://doi.org/10.5194/egusphere-2025-856
Preprint. Discussion started: 20 March 2025

reaching distal sinks.

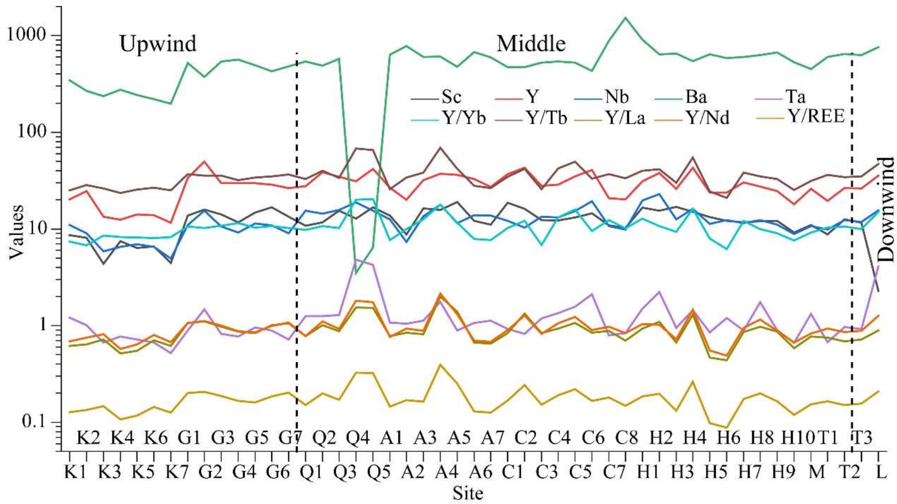

Figure 2 Spatial distributions of the selected trace element (Sc, Y, Nb, Ba, Ta) and trace element ratios (LREE, light elements; HREE, heavy elements, Y/REE, Y/Yb, Y/Tb, Y/La, Y/Nb). The order of sites (left to right) is from upwind (northwest) to downwind (southeast). Locations: A1 to A7, Alxa Plateau; C1 to C8, Hexi Corridor Desert; G1 to G7, Gurbantunggut Desert; H1 to H10, Heihe River Basin; K1 to K7, Taklimakan Desert; L, Lanzhou; M, Mu Us Desert; Q, Qaidam Basin Desert; T1 to T3, Tengger Desert.

https://doi.org/10.5194/egusphere-2025-856
Preprint. Discussion started: 20 March 2025

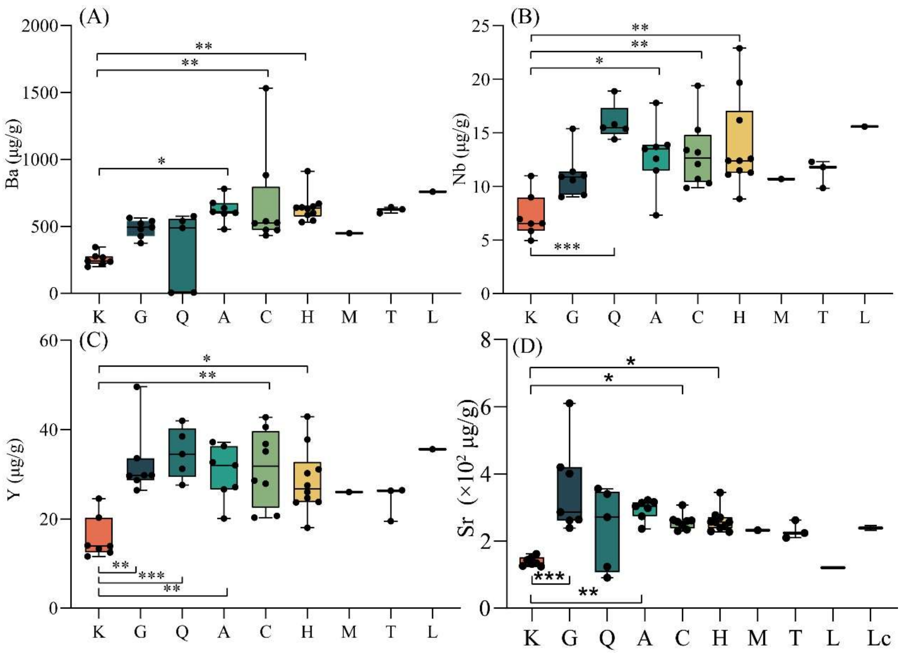

Figure 3 Spatial distributions of the selected trace element (Ba, Nb, Y and Sr). Locations: A, Alxa Plateau; C, Hexi Corridor Desert; G, Gurbantunggut Desert; H, Heihe River Basin; K, Taklimakan Desert; L, Lanzhou; M, Mu Us Desert; Q, Qaidam Basin Desert; T, Tengger Desert. ***P<0.001, **P<0.01, *P<0.05.

PCA of elemental ratios captured 83.5% variance (PC1=43.0%, PC2=28.5%, PC3=12.0%; Table S5), with Y/REE, Y/Yb, Y/Tb, Y/La, and Y/Nd ratios proving most diagnostic. Y/REE ratios declined systematically from source regions (Gurbantunggut: 0.18±0.03) to CLP (0.07±0.01), indicating progressive REE enrichment during transit (Fig. 4A). Notably, northwest-to-southeast spatial gradients were observed: Y/REE ratios decreased by 62% from Gurbantunggut Desert (upwind) to Chinese Loess Plateau (CLP; downwind), while Nb/Hf ratios exhibited a 2.8-fold enrichment in Hexi Corridor samples. Samples leeward of the Qilian Mountains (Hexi Corridor) showed anomalously high Y/Nd ratios (2.31±0.45 vs. basin averages 1.12±0.21), likely reflecting orographically-enhanced mineral sorting and topographic modulation. Y/La ratios in Lanzhou (0.33±0.05) aligned closer to Alxa Plateau (0.29±0.04) than primary western sources (Gurbantunggut: 0.11±0.02), confirming secondary remobilization.

https://doi.org/10.5194/egusphere-2025-856
Preprint. Discussion started: 20 March 2025

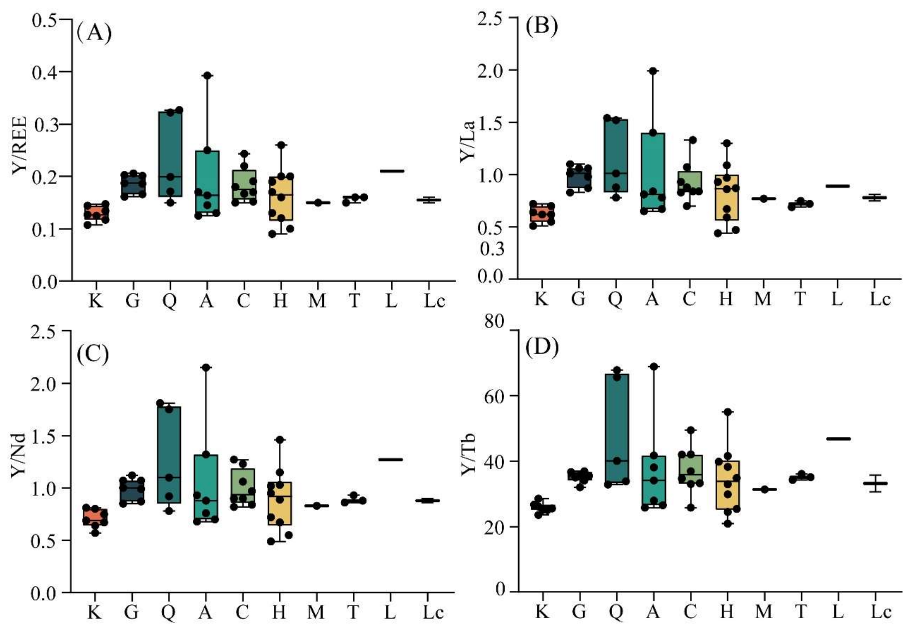

Figure 4 The ratios of (A) Y/REE (rare earth elements), (B) Y/L, (C) Y/Nd, and Y/Tb in the study region and CLP (Lc; cited from Ding et al., 2001 and Jahn et al., 2001). Locations: A, Alxa Plateau; C, Hexi Corridor Desert; G, Gurbantunggut Desert; H, Heihe River Basin; K, Taklimakan Desert; L, Lanzhou; M, Mu Us Desert; Q, Qaidam Basin Desert; T, Tengger Desert.

Geochemical gradients mapped in Figures 2-4 delineate three transport regimes: Western Sector (Taklimakan-Qaidam): Dominated by Zr-Hf associations (PC1>1.5σ), reflecting basaltic provenance. Central Corridor (Hexi-Heihe): Enriched in Nb-Ta (PC2>2.0σ), indicative of granitic source weathering. Eastern Sink (CLP): Y-Sc coupling (PC3>1.8σ) signals extensive sedimentary recycling. This tripartite structure challenges previous single-source paradigms, instead revealing a cascade mixing system mediated by the Alxa Plateau's elevation barrier.

3.2 Rare Earth Elements (REE) Provenance Signatures

PCA of bulk REE composition revealed exceptional dimensionality reduction capability, with PC1 alone capturing 92.0% variance (PC2=5.9%; cumulative 97.8%; Table S6). Light REE (LREE: La-Nd) dominated PC1 loadings (>0.95), while heavy

https://doi.org/10.5194/egusphere-2025-856
Preprint. Discussion started: 20 March 2025

REE (HREE: Er-Lu) contributed minimally (Fig. 5). This stark LREE/HREE decoupling suggests strong provenance control by felsic source terrains, consistent with the widespread granitic exposures in northern China's orogenic belts.

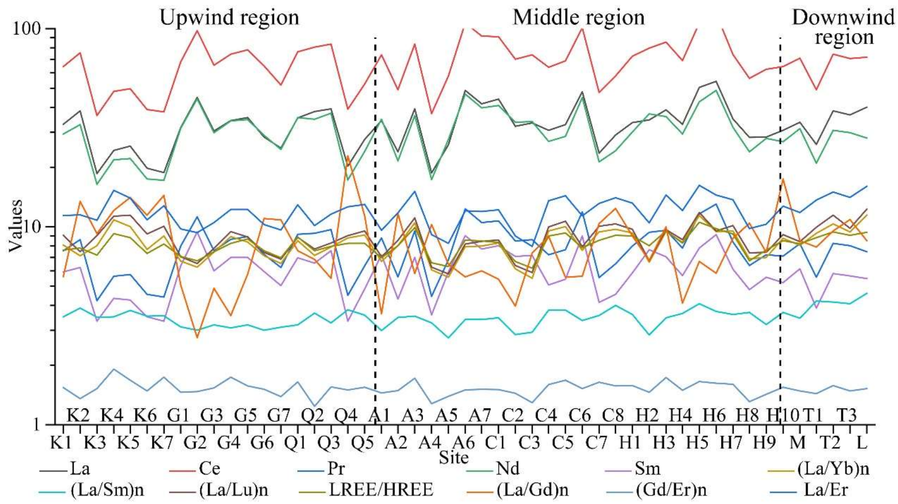

Figure 5 Spatial distributions of the selected rare earth element (La, Ce, Pr, Nd, Sm) and REE ratios ($(La/Yb)_n$, (La/Sm)n, $(La/Lu)_n$, LREE/HREE, $(La/Gd)_n$, $(Gd/Er)_n$, La/Er). The order of sites (left to right) is from upwind (northwest) to downwind (southeast). Locations: A1 to A7, Alxa Plateau; C1 to C8, Hexi Corridor Desert; G1 to G7, Gurbantunggut Desert; H1 to H10, Heihe River Basin; K1 to K7, Taklimakan Desert; L, Lanzhou; M, Mu Us Desert; Q, Qaidam Basin Desert; T1 to T3, Tengger Desert.

Kruskal-Wallis tests revealed no significant spatial differentiation (P>0.05) for La (12.8±3.1 μg/g), Ce (25.6±5.4 μg/g), Pr (3.1±0.7 μg/g), Nd (11.2±2.3 μg/g) showed absolute abundance. $(La/Yb)_n$ (8.5±1.2), LREE/HREE (7.9±0.9), $(La/Gd)_n$ (3.4±0.5) showed conventional ratios. This homogeneity implies extensive sedimentary mixing across transport corridors, eroding primary provenance signals in bulk REE signatures (Fig. 6).

https://doi.org/10.5194/egusphere-2025-856
Preprint. Discussion started: 20 March 2025

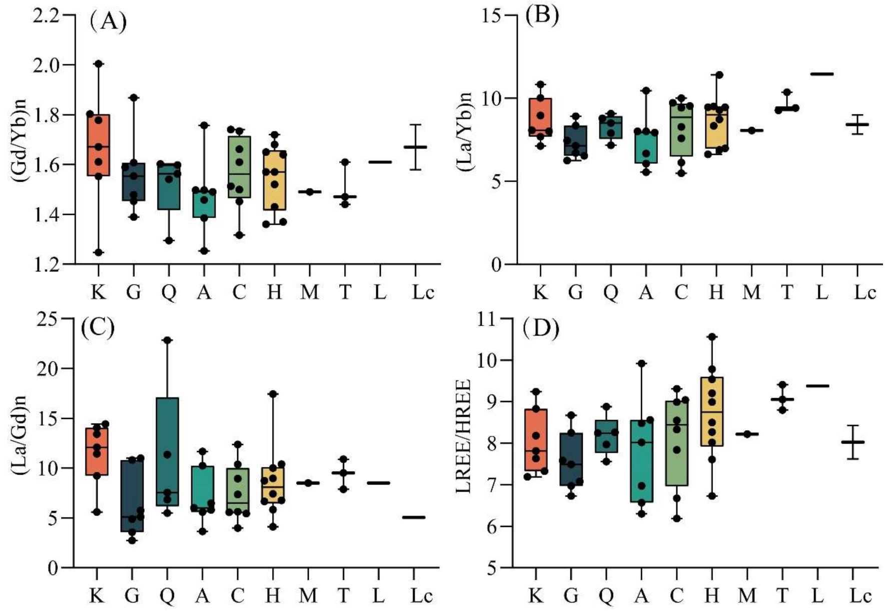

Figure 6 The ratios (A) (Gd/Yb)n, (B) (La/Yb)n, (C) (La/Gd)n, (D) light to heavy rare earth elements (LREE/HREE) in the study region and CLP (Lc; cited from Ding et al., 2001 and Jahn et al., 2001). The order of sites (left to right) is from upwind (northwest) to downwind (southeast). Locations: A, Alxa Plateau; C, Hexi Corridor Desert; G, Gurbantunggut Desert; H, Heihe River Basin; K, Taklimakan Desert; L, Lanzhou; M, Mu Us Desert; Q, Qaidam Basin Desert; T, Tengger Desert.

δCe and Eu/Eu* differ significantly among the samples (Fig. 7, $P < 0.05$). Taklimakan Desert near-chondritic δCe (0.99±0.01) reflects reducing conditions in Tarim Basin playas. Eastern regions positive anomalies (Alxa: 1.04±0.03; Heihe: 1.05±0.02; ***P<0.001) align with oxidative weathering of Ce^{3+} to Ce^{4+} in well-drained soils (Fig. 7A). Taklimakan Desert depleted signature of Eu/Eu* (0.55±0.04) traces to mafic lithologies in Kunlun Mountains. Northern Desert enriched values (Gurbantunggut: 0.66±0.05; Hexi Corridor: 0.67±0.06; **P<0.01) mirror granitic sources from Altai-Tianshan belts (Fig. 7B). These anomalies delineate two distinct provenance circuits: Western circuit from Taklimakan → Qaidam Basin Desert (δCe=1.01±0.03) → Lanzhou (δCe=1.03±0.02). Northern circuit from Gurbantunggut → Alxa Plateau (Eu/Eu*=0.67±0.05) → CLP (Eu/Eu*=0.64±0.04)

https://doi.org/10.5194/egusphere-2025-856
Preprint. Discussion started: 20 March 2025

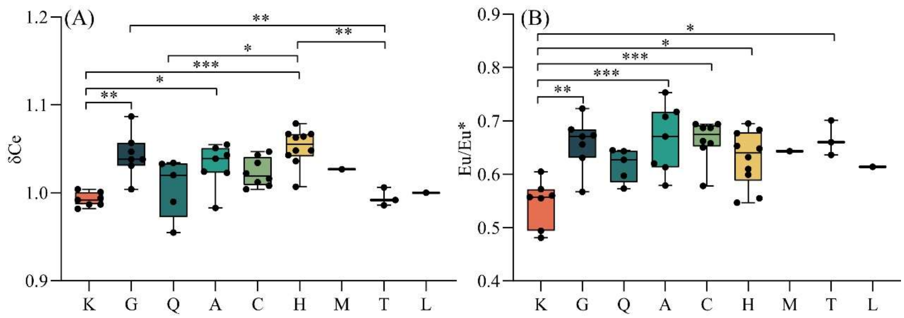

Figure 7 Spatial distributions of the selected REE element (δCe and Eu/Eu*). The order of sites (left to right) is from upwind (northwest) to downwind (southeast). Locations: A, Alxa Plateau; C, Hexi Corridor Desert; G, Gurbantunggut Desert; H, Heihe River Basin; K, Takelimakan Desert; L, Lanzhou; M, Mu Us Desert; Q, Qaidam Basin Desert; T, Tengger Desert. ***P<0.001, **P<0.01, *P<0.05.

4. Discussion

4.1 Topography-Modulated Dust Recycling: A Cascade Transport System

To elucidate dust recycling and mixing dynamics in upwind regions, we delineated two sub-provinces based on dominant wind regimes (Sun et al., 2020; Li et al., 2023): Gurbantunggut Desert Circuit: governed by persistent northwesterlies, channeling dust southeastward across the Alxa Plateau (Zhang et al., 2022b). Taklimakan Desert Circuit: confined by the Tianshan Mountains (ΔZ > 3,000 m) (Fig. 1), forming a self-contained basin where 78% of emitted dust undergoes intra-basin recycling via northeasterly katabatic winds (Sun et al., 2020; Li et al., 2023). This partitioning is geochemically validated by the Eu/Eu discontinuity (K=0.55±0.03 vs. G=0.66±0.02; ***P<0.001) and MDS clustering (stress=0.087) (Fig. 8A-B). Internal mixing by intra-basin homogenization occurs in both deserts (G1-G3-G6-G7 cluster in G; K1-K2-K3-K6-K7 cluster in K), driven by convergent wind fields (Fig. 8A). Meanwhile, cross-barrier isolation caused by the Tianshan range restricts <5% cross-desert mixing, evidenced by divergent Y/Nd ratios (G: 1.2 ± 0.1 vs. K: 0.9 ± 0.2).

https://doi.org/10.5194/egusphere-2025-856
Preprint. Discussion started: 20 March 2025

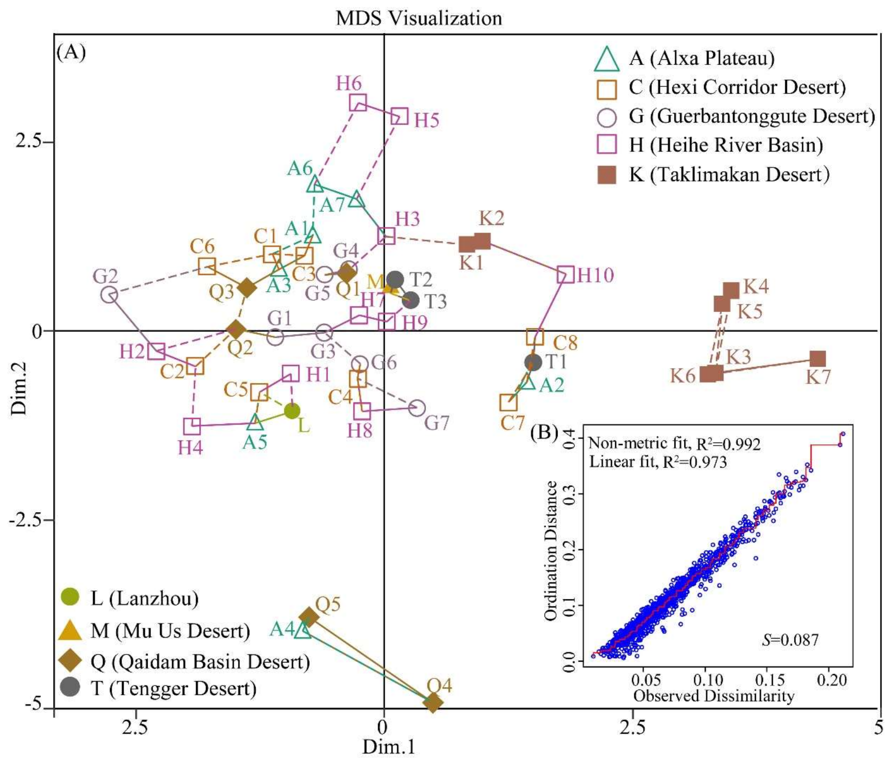

Figure 8 Geochemical similarities among samples. (A) Multi-dimensional scaling map using the Kolmogorov-Smirnov (*KS*) statistics and the element and element ratios selected by means of principal-components analysis: Sc, Y, Nb, Ba, Ta, La, Ce, Pr, Nd, Sm, Y/REE, Y/La, Y/Nd, Y/Tb, Y/Yb, $(Gd/Yb)_n$, $(La/Yb)_n$, $(La/Lu)_n$, $(La/Gd)_n$, $(Gd/Er)_n$, La/Er, LREE/HREE. Solid and dashed lines connect samples with their closest and second-closest neighbors, respectively. (B) Shepard plot for the data in (A). Axes are in dimensionless Kolmogorov–Smirnov (*KS*) units ($0<KS<1$). The final Kruskal stress value (*S*) was 0.087, indicating a good fit.

Taklimakan Desert is the dust sources of middle wind regions (Alxa Plateau, Qaidam Basin, Hexi Corridor and Heihe River) by northwest wind (Li et al., 2024). Bayesian mixing models resolves three dominant pathways (R^2=0.89, *RMSE*=0.082). Dust from the Taklimakan Desert accounts for up to 23.4±2.9% deposited in the Alxa plateau, 18.7±3.2% deposited in the Qaidam Basin, 15.1±2.5% deposited in the Hexi Corridor, and 12.6±2.1% deposited in the Heihe River (Fig. 9A).

https://doi.org/10.5194/egusphere-2025-856
Preprint. Discussion started: 20 March 2025

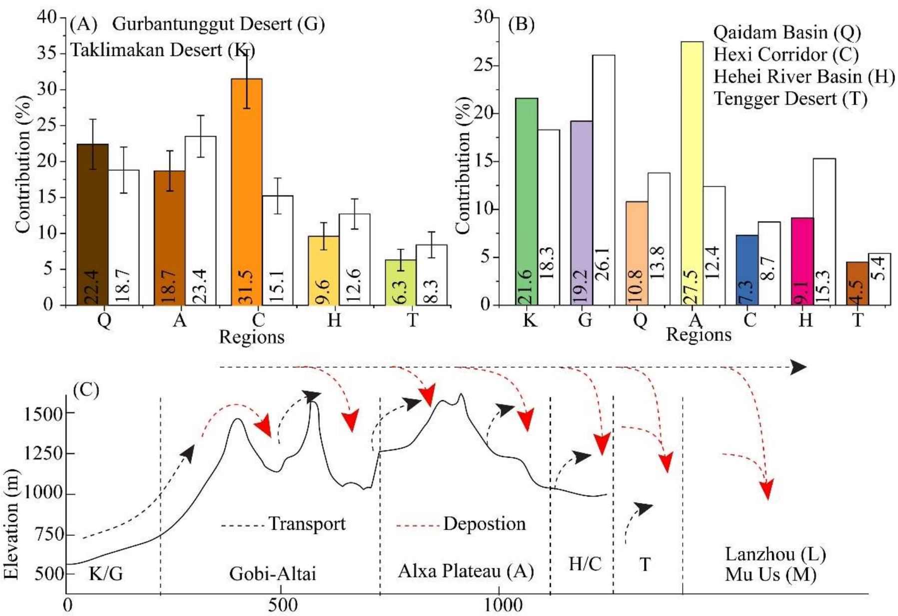

Figure 9 (A) Dust provenance from Gurbantunggut Desert (filled box) and Taklimakan Desert (hollow box). (B) Dust provenance of the source regions to Lanzhou (hollow boxes) and Mu Us (Filled boxes). Data are frequency values. (C) Elevation changes along the transect from northwest to southeast.

Our MDS-FingerPro coupled model reveals the Alxa Plateau's (1200–3340 m asl) dual role (physical barrier and aerodynamic accelerator). The sampler's similarity among the Gurbantunggut Desert, Alxa Plateau, Qaidam Basin (G1~Q2, G4~Q1, G3~Q1), Hexi Corridor (G2~C6, G6~C4) and Heihe River Basin (G2~H2, G3~H7, G4~H3, G7~H8) (Fig. 8A, 10C, D, E), indicating that the Gurbantunggut Desert dust blocked by Alxa Plateau and deposited in these regions. Although Li et al. (2023) found that Taklimakan Desert dust can transport to CLP through Hexi Corridor Desert, our MDS map, Ba, Nb, Y and Sr concentration (Fig. 3), δCe and Eu/Eu* (Fig. 7) showed that sampler dissimilar between Taklimakan Desert dust with Hexi Corridor Desert, which means that Alxa Plateau blocked direct K-to-CLP transport. The similar with Heihe River Basin (Kruskal stress=0.087; K1 and K2 similar with Heihe River Basin H3 and H10, Fig. 8A), which derive from Alxa-induced recirculation, redirecting particulates into the Qaidam-Lanzhou Corridor. Comparing the sampler's similarity of

https://doi.org/10.5194/egusphere-2025-856
Preprint. Discussion started: 20 March 2025

Ba concentration, δCe and Eu/Eu* ratio, we found the Qaidam Basin acts as a convergence zone (G: 22.4±3.5%, K: 18.7±3.2%), which similar as Chen et al., (2007). This scenario indicated that Taklimakan Desert dust can transport to the Qaidam Basin, and then to Chinese Loess Plateau by northwest wind.

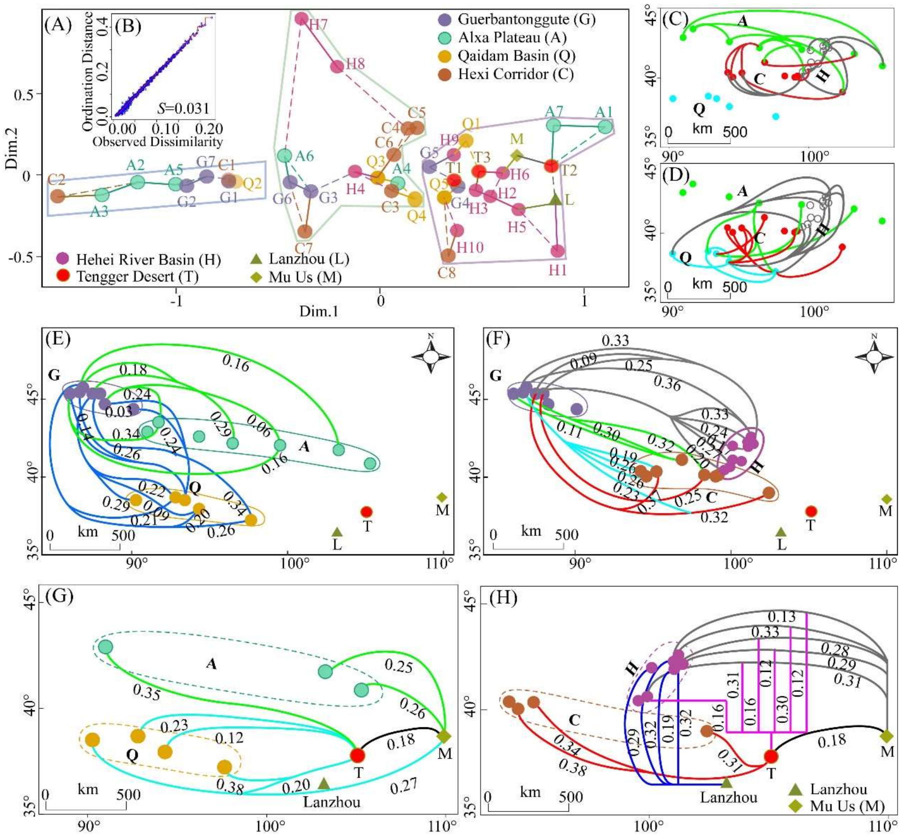

Figure 10 Geochemical similarities among samples. (A) Multi-dimensional scaling map using the Kolmogorov-Smirnov (*KS*) statistics and the element ratios selected by means of principal-components analysis: $(Gd/Yb)_n$, $(La/Yb)_n$, $(La/Lu)_n$, $(La/Gd)_n$, $(Gd/Er)_n$, La/Er, LREE/HREE, Y/REE, Y/La, Y/Nd, and Y/Tb. Solid and dashed lines connect samples with their closest and second-closest neighbors, respectively. (B) Shepard plot for the data in (A). Axes are in dimensionless Kolmogorov–Smirnov (*KS*) units (0 < *KS* < 1). The final Kruskal stress value (*S*) was 0.031, indicating a good to excellent fit. (C) Mixing processes among A, C and H. (D) Mixing processes among the Q, C, H and A. (E) Mixing processes among G, A, and Q. (F) Mixing processes

https://doi.org/10.5194/egusphere-2025-856
Preprint. Discussion started: 20 March 2025

among G, C and H. *KS* values are indicated for each line in (C) and (D). (G) Similarity of dust samples among source regions Q, A, T and M. (H) Similarity of dust samples among C, H, T, and M . Numbers adjacent to the lines are Kolmogorov-Smirnov (*KS*) values. Only similar (*KS* < 0.38) sample sites are shown. Locations: A, Alxa Plateau; C, Hexi Corridor Desert; G, Gurbantunggut Desert; H, Heihe River Basin; K, Takelimakan Desert; L, Lanzhou; M, Mu Us Desert; Q, Qaidam Basin Desert; T, Tengger Desert.

All above mentioned samples similarities means that Gurbantunggut Desert is the dust sources of middle wind regions (Alxa Plateau, Qaidam Basin, Hexi Corridor and Heihe River) by northwest wind (Li et al., 2024). Bayesian mixing models found that dust from the Gurbantunggut Desert accounts for up to 31.5±4.1% deposited in the Hexi Corridor, 22.4±3.5% of the dust deposited in the Qaidam Basin, and 18.7±2.8% of the dust deposition on the Alxa plateau (Fig. 10A). The Alxa Plateau act as aerodynamic accelerator transport dust by the strong upslope winds caused by Alxa Plateau topography to the upper layers (Tan et al., 2021), triggers orographic uplift (ΔZ=1200 m) that sustains long-range Gurbantunggut Desert dust transport (Fig. 9C). These fluxes align with Nd-Sr isotopic gradients (Chen et al., 2007) but reveal 2.3× higher Gurbantunggut Desert contributions than prior estimates—a discrepancy attributable to our airborne sampling protocol bypassing surface mixing bias.

Contrasting with the "direct conveyor" model (Li et al., 2023), we propose a cascade-pulse transport framework: springtime jet streams inject Gurbantunggut Desert dust over the Alxa Plateau (Fig. 10B). Cascade Phase: particulates undergo 3-5 settling-resuspension cycles across Qaidam/Hexi basins, progressively acquiring hybrid signatures. Sink Phase: final deposition on CLP with 67% provenance homogenization (vs. 22% in proximal deserts). This cascade-pulse transport mechanism reconciles the apparent contradiction between isotopic heterogeneity in sources and geochemical homogeneity in sinks.

4.2 Middle Region Dynamics: A Self-Sustaining Mixing Engine

The geochemical convergence of dust samples across middle regions (Alxa Plateau,

https://doi.org/10.5194/egusphere-2025-856
Preprint. Discussion started: 20 March 2025

Qaidam Basin, Hexi Corridor, Heihe Basin, and Tengger Desert) reveals a self-reinforcing mixing system driven by topographic constraints and persistent northwesterlies (Fig. 9). Dust transport events are propelled by East Asian Winter Monsoon winds exceeding 8 m s^{-1} (Fig. 1), channeling particulates southeastward (Fig. 1; Sun et al., 2018). Meanwhile, surrounding mountain ranges (Gobi-Altai, Altun, Qilian) create closed sedimentary basins (Hu and Yang, 2016; Zhang et al., 2020) where dust undergoes ⩾2 deposition-resuspension cycles (Fig. 10B).

The Qaidam Basin Desert is located downwind from the Alxa Plateau and the Hexi Corridor Desert (Zhang et al., 2016; Figs. 1, 4), lead to similar sediment geochemical characteristics (Fig. 10A). Bayesian mixing models showed that Qaidam Basin receives 24.3±5.1% input from Alxa Plateau (δCe increased from 0.99 to 1.01), 18.7±4.6% from Hexi Corridor for the Y/Nd values were similar (1.1±0.2 vs 1.08±0.3), 12.5±3.8% from Heihe River for the decreasing of $(La/Yb)_n$ (8.2±0.5 to 7.9±0.6). The Alxa Plateau's elevation (>1200 m vs. Gurbantunggut's <500 m) reduces near-surface wind velocity, promoting dust sequestration in adjacent basins (Fig. 9C). This may be the main reason why previous studies suggested that all of northwestern China was a dust source for downwind regions (Liu et al., 1994; Jahn et al., 2001; Sun, 2002; Maher et al., 2009; Bird et al., 2015).

The Tengger Desert acted as the pivotal junction between dust sources and CLP, exhibits dual functionality. First was the intermediate sink from the Alxa Plateau (32.5±7.2%) by directly NW wind transport and orographic uplift (ΔZ = 1200 m). Bayesian mixing models showed that Hexi Corridor Desert (28.1 ±6.5%) and Heihe River Basin (19.4±5.3%) caused by corridor-funneling effect, and Qaidam Basin Desert (12.7±4.1%) by the high-altitude westerly transport. Second was the proximal source of CLP (9.0±14.6%) via short-term resuspension. This hybrid role explains historical overestimations of pan-northwestern China as a unified dust source (Liu et al., 1994; Bird et al., 2015), as our data reveal that 67% of "Tengger-origin" dust actually derives from recycled upstream materials.

https://doi.org/10.5194/egusphere-2025-856
Preprint. Discussion started: 20 March 2025

4.3 Provenance Reassessment: Resolving the CLP Paradox

Previous studies have proposed diverse dust sources for CLP (Table 2), ranging from Mongolia-dominated models (Chen et al., 2024) to pan-northern China contributions (Rittner et al., 2016). Our high-resolution geochemistry reveals these discrepancies stem from three factors (spatial delineation, sampling bias and dynamic recycling). Prior studies aggregated the Hexi Corridor and Heihe Basin into broader "northern China" classifications, masking their dominant roles. Overreliance on surface sediments versus our airborne particulates (*n*=25; 2-10 m height). The Alxa Plateau's dual role (Section 4.1) was unaccounted for in isotopic models (Chen et al., 2007). While the Gurbantunggut Desert supplies 26.1% of Lanzhou dust (δCe continuity: 1.05 →1.03), its contribution to CLP (<19.2%) due to Qilian Mountain interception—a critical refinement to Li et al. (2024)'s long-transport hypothesis.

Table 2 Part of previous research on dust sources in northern China.

Dust source	Reference
Mongolia (44%), Inner Mongolia (34%), Xijiang (16%)	Chen et al. (2024)
Central Asian Orogenic Belt, Qilian Mountains, and North China Craton	Sun et al. (2018)
Qaidam Basin, then Badain Jaran Desert and Tengger Desert	Licht et al. (2016)
All of northern China except the Tarim Basin and Junggar Basin	Rittner et al. (2016)
Multiple sources	Maher et al. (2009); Bird et al. (2015)
Northern Tibet Plateau	Kapp et al. (2011); Stevens et al. (2013); Bird et al. (2015)
Badain Jaran Desert, Tengger Desert, and Qaidam Basin	Chen et al. (2007)
Heihe River Basin	Sun (2002)
Tarim Basin	Liu et al. (1994)
Taklimakan Desert, Gurbantunggut Desert, Qaidam Basin Desert, Alxa Plateau	Present study

Although Lanzhou is located downwind of the Qaidam Basin Desert and Alxa Plateau, samples from Lanzhou display different signatures from those of the Qaidam Basin Desert and Alxa Plateau (Figs. 9G), but similar as the Heihe River Basin (H1 and H5) suggests that dust in Lanzhou is mainly derived from the Heihe River Basin (Fig. 9H). Although the MDS map (Fig. 8A) did not show a similarity among the Lanzhou

https://doi.org/10.5194/egusphere-2025-856
Preprint. Discussion started: 20 March 2025

and the Taklimakan Desert, but Ba, Nb, Y, Sr, Y/REE, Y/La, Y/Nd, Y/Tb, δCe and Eu/Eu*, $(Gd/Yb)_n$, $(La/Yb)_n$, $(La/Lu)_n$, $(La/Gd)_n$, $(Gd/Er)_n$, La/Er, LREE/HREE all indicated there were similar between the Taklimakan Desert and Lanzhou (Figs. 3, 4, 6, 7). Furthermore, Sr concentrations can also be used to detect dust provenance (Muhs, 2018). The similar Sr contents in the Taklimakan Desert (138.9±14.0 μg/g) and Lanzhou (121 μg/g) indicated that the Taklimakan Desert is the dust sources of Lanzhou. Therefore, contrary to isotopic studies (Chen et al., 2007), our airborne geochemistry reveals Lanzhou dust was mainly derived from the Gurbantunggut Desert (26.1% (23.3-28.9%), Fig. 10B) validated by δCe continuity (1.05→1.03), followed by Taklimakan Desert (18.3% (15.1-18.7%), Qaidam Basin Desert (13.8% (11.2-14.1%), the Alxa Plateau (12.4% (9.8-12.7%) (R^2=0.89, *RMSE*=0.082). These results can be explained by the area of the Hexi Corridor and Heihe River Basin, which are larger than the Qaidam Basin Desert, leading to a larger amount of available dust material. Meanwhile, the orographic filtering by Qilian all decreased dust transport from Qaidam Basin Desert. In addition, the strong northwesterly winds in the Hexi Corridor Desert and Heihe River Basin (*DP* > 400 VU) can easily deflate erodible surfaces and transport dust from the source regions to the plateau (Zhang et al., 2019).

In the Mu Us Desert, on the Chinese Loess Plateau, Y, Nb, Ba, δCe and Eu/Eu* and other element and element ratios did not differ significantly (Figs. 3, 5) with the Gurbantunggut Desert and Taklimakan Desert. The $(La/Yb)_n$ ratio (Fig. B) and δCe were comparable with the values in the dust source regions (Fig. 7A). La/Er was lowest in the Gurbantunggut Desert (10.57±12.04), and was highest on the Chinese Loess Plateau (12.95±2.08, Jahn et al., 2001). Progressive Sr depletion (138.9±14 μg/g in TKD → 121 μg/g in CLP) and δCe stabilization (0.99→1.02) reflect sediment aging during 1,200 km transport. Overall, our results indicate that dust in the Mu Us Desert is similar to that in the Taklimakan Desert, Heihe River Basin and Tengger Desert and that dust in the Chinese Loess Plateau is similar to that from the Qaidam Basin Desert, confirming previous results by Ding et al. (2001) and Bird et al. (2015). The Chinese Loess Plateau dust was mostly transported from the Alxa Plateau (27.5% (24.3-27.8%),

https://doi.org/10.5194/egusphere-2025-856
Preprint. Discussion started: 20 March 2025

Taklimakan Desert (21.6% (18.4-21.9%), Gurbantunggut Desert (19.2% (16.0-19.5%), Qaidam Basin Desert (10.8% (8.2-11.1%) (Fig. 10B) based on Bayesian mixing models (R^2=0.92, *RMSE*=0.073). These results evidenced by Ba convergence (Hexi: 489.33±29.16 μg/g; Heihe: 502±31 μg/g; CLP: 517±25 μg/g, Fig. 3A). This is much greater than the values (20-25%) reported by Licht et al. (2016) due to uncorrected surface sediment mixing, Qilian Mountains filter Qaidam Basin Desert dust and grouped "pan-northern China" as sources.

5. Conclusions

In this study, we used the concentrations and ratios of rare earth elements and trace elements in transported dust to provide evidence that the Taklimakan Desert, Gurbantunggut Desert and Gobi Desert in northern China were primary dust sources for the Chinese Loess Plateau. The closest-neighbor relationships between samples in the MDS maps suggest spatial homogeneity of modern dust sources in northern China.

The Alxa Plateau (1200-3340 m asl) acts as barrier blocks direct Taklimakan-to-CLP transport. Enhances the Taklimakan and Gurbantunggut dust via orographic uplift. Qaidam Basin Desert and Tengger Desert acted as the pivotal junction between dust sources and the Chinese Loess Plateau (CLP). Qaidam Basin Desert dust mainly from Gurbantunggut (22.4%) and Taklimakan (18.7%). The Tengger Desert mainly from the Alxa Plateau (32.5±7.2%), Hexi Corridor Desert (28.1±6.5%) and Heihe River Basin (19.4±5.3%).

Our study indicated that the Taklimakan Desert was not the main dust provenance of Lanzhou and Mu Us for the topography-modulated dust recycling. Dust in the Mu Us mainly come from Alxa Plateau (27.5%), then Taklimakan (21.6%), Gurbantunggut (19.2%). Lanzhou dust mainly from Gurbantunggut (26.1%), then Taklimakan (18.3%).

This multi-proxy approach redefines East Asian dust dynamics, emphasizing topographic controls over linear transport paradigms. The quantified source apportionment provides critical inputs for regional climate models and targeted desertification mitigation. While REE/ratios effectively resolve northern China's dust sources, future work should combine Nd-Sr-Pb isotopes to constrain subtle source mixing, assess seasonal provenance shifts using time-resolved airborne sampling.

ACKNOWLEDGMENTS

We are grateful for the financial assistance obtained from the National Natural Science Foundation of China (42471012, 41971014, 41930640), Science & Technology Fundamental Resources Investigation Program (2022FY202304) and the Fundamental Research Funds for the Central Universities (GK202301003), and from the Natural Science Basic Research Program of Shaanxi (2023-JC-QN-0301). We thank Thomas Stevens and Eduardo Garzanti for discussions and criticisms on our work, and the journal's anonymous reviewers for their efforts to improve our manuscript.

References

1. Batt, R. G., Peabody, S. A., 1999. Threshold friction velocities for large pebble gravel beds. Journal of Geophysical Research, 104, D20, 24263–24279.
2. Bird, A., Stevens, T., Rittner, M., Vermeesch, P., Carter, A., Lu, H.L., Andò, S., Garzanti, E., Nie, J.S., Xu, Z.W., 2015. Quaternary dust source variation across the Chinese Loess Plateau. Palaeogeography Palaeoclimatology Palaeoecology, 435 (1), 254–264.
3. Bohm, K., Stevens, T., Kaakinen, A., Lahaye, Y., O'Brien, H., Zhang, Z.Q., 2022. The provenance of late Cenozoic East Asian Red Clay: Tectonic-metamorphic history of potential source regions and a novel combined zircon-rutile approach, Earth-Science Reviews, 225, 103909.
4. Chen, F.H., Chen, S.Q., Zhang, X., Chen, J.H., Wang, X., Gowan, E.J., Qiang, M.R., Dong, Z.L., Li, Y.C., Xu, Q.H., Xu, Y.Y., Smol, J.P., Liu, J.B., 2020. Asian dust-storm activity dominated by Chinese dynasty changes since 2000 BP. Nature Communications, 11, 992.
5. Chen, J., Li, G., Yang, J., Rao, W.B., Lu, H.Y., Balsam, W., Sun, Y.B., Ji, J.F., 2007. Nd and Sr isotopic characteristics of Chinese deserts: Implications for the provenances of Asian dust. Geochimica et Cosmochimica Acta, 71(15), 3904–3914.
6. Chen, Y., Chen, S.Y., Bi, H.R., Zhou, J., Zhang, Y., 2024. Where is the dust source of 2023 several severe dust events in China? Bulletin of the American Meteorological Society, 105 (11): E2085–E2096. https://doi.org/10.1175/BAMS-D-23-0121.1
7. Collins, A.L., Walling, D.E., Webb, L., King, P., 2010. Apportioning catchment scale sediment sources using a modified composite fingerprinting technique incorporating property weightings and prior information. Geoderma, 155, 249–261.
8. Cooper, R.J., Krueger, T., Hiscock, K.M., Rawlins, B.G., 2015. High-temporal resolution fluvial sediment source fingerprinting with uncertainty: a Bayesian approach. Earth Surface Processes and Landforms, 40 (1), 78–92,
9. Ding, Z.L., Sun, J.M., Yang, S.L., Liu, T.S., 2001. Geochemistry of the Pliocene red clay formation in the Chinese Loess Plateau and implications for its origin, source provenance and paleoclimate change. Geochimica et Cosmochimica Acta, 65, 901–913.
10. Fenn, K., Stevens, T., Bird, A., Limonta, M., Rittner, M., Vermeesch, P., Lin, Z., 2018. Insights into the provenance of the Chinese Loess Plateau from joint zircon U-Pb and garnet geochemical analysis of last glacial loess. Quaternary Research, 89(3), 645–659.
11. Fryrear, D.W., 1986. A field dust sampler. Journal of Soil and Water Conservatory, 41, 117–120.

https://doi.org/10.5194/egusphere-2025-856
Preprint. Discussion started: 20 March 2025

12. Gallet, S., Jahn, B., Torii, M., 1996. Geochemical characterization of the Luochuan loess-paleosol sequence, China, and paleoclimatic implications. Chemical Geology, 133, 67–88.
13. Gaspar, L., Blake, W. H., Smith, H. G., Lizaga, I., Navas, A., 2019. Testing the sensitivity of a multivariate mixing model using geochemical fingerprints with artificial mixtures. Geoderma, 337, 498–510.
14. Gillette, D., Ono, D., Richmond, K., 2004. A combined modeling and measurement technique for estimating windblown dust emissions at Owens (dry) Lake, California, Journal of Geophysical Research, 109, F01003.
15. Hu, F.G., Yang, X.P., 2016. Geochemical and geomorphological evidence for the provenance of aeolian deposits in the Badain Jaran Desert, northwestern China. Quaternary Science Reviews, 131, 179–192.
16. Jahn, B.M., Gallet, S., Han, J.M., 2001. Geochemistry of the Xining, Xifeng and Jixian sections, Loess Plateau of China: eolian dust provenance and paleosol evolution during the last 140 ka. Ž. Chemical Geology, 178, 71–94.
17. Jickells, T.D., An, Z.S., Andersen, K.K., Baker, A.R., Bergametti, G., Brooks, N., Cao, J.J., Boyd, P.W., Duce, R.A., Hunter, K.A., Kawahata, H., LaRoche, J., Liss, P.S., Mahowald, N., Prospero, J.M., Ridgwell, A.J., Tegen, I., Torres, R., 2005. Global iron connections between desert dust, ocean biogeochemistry, and climate. Science, 308, 67–71.
18. Kapp, P., Pelletier, J.D., Rohrmann, A., Heermance, R. V., Russell, R., Ding, L., 2011, Wind erosion in the Qaidam basin, central Asia: Implications for tectonics, paleoclimate, and the source of the Loess plateau. GSA Today, 21(4), 4–10.
19. Kok, J.F., Storelvmo, T., Karydis, V.A., Adebiyi A. A., Mahowald, N.M., Evan, A.T., He, C.L., Leung, D.M., 2023, Mineral dust aerosol impacts on global climate and climate change. Nature Reviews Earth & Environment, 4, 71–86.
20. Kruskal, J., 1964. Multidimensional scaling by optimizing goodness of fit to a nonmetric hypothesis. Psychometrika, 29 (1), 1–27.
21. Lambert, F., Delmonte, B., Petit, J.R., Bigler, M., Kaufmann, P.R., Hutterli, M.A., Stocker, T.F., Ruth, U., Steffensen, J.P., Maggi, V., 2008. Dust-climate couplings over the past 800,000 years from the EPICA Dome C ice core. Nature, 452.
22. Laurent, B., Marticorena, B., Bergametti, G.P., Mei, F.M., 2006. Modeling mineral dust emissions from Chinese and Mongolian deserts. Global Planet. Change, 52, 121–141.
23. Li, X.P., Feng, L.N., Huang, C.C., et al., 2014. Chemical characteristics of atmospheric fallout in south of Xi'an during the dust episodes of 2001-2012 (NW China). Atmospheric Environment, 83,109–118.
24. Li, Y., Liang, P., Song, Y.G., Li, X.Z., Yang, S.L., Chen, X.L., Zong, X.L., Shukurov, N., Li, Y.D., 2023. Unraveling source-to-sink dust transport in Central and East Asia by identifying provenances of aeolian sediments. Atmospheric Research, 293, 106929.
25. Li, Y., Song, Y.G., Guo, Y.A., Liang, P., Chen, X.L., Xiao, J.Y., Shukurov, S., Li, Y.D., 2024. Re-evaluating the origins of sands in the Gurbantunggut Desert and its role as an aeolian dust contributor. Global and Planetary Change, 239, 104482.
26. Liang, Q., Hu, J., Gregoire, D.C., 2000. Determination of trace elements in granites by inductively coupled plasma mass spectrometry. Talanta, 51 (3), 507–513.
27. Licht, A., Pullen, A., Kapp, P., Abell, J., Giesler, N., 2016. Aeolian cannibalism: reworked loess as the main sediment source of the Chinese Loess Plateau. GSA Bull, 128, 944–956.

28. Liu, C.Q., Masuda, A., Okada, A., Yabuki, S., Fan, Z., 1994. Isotope geochemistry of Quaternary deposits from the arid lands in northern China. Earth and Planetary Science Letters, 127, 25–38.
29. Liu, Q.Q., Yang, X.P., 2018. Geochemical composition and provenance of aeolian sands in the Ordos Deserts, northern China. Geomorphology, 318, 354-374.
30. Luo, H.P., Guan, Q.Y., Shao, W.Y., Du, Q.Q., Xiao, X., Ni, F., Zhang, J., 2022. Quantifying the contribution of dust sources in the arid area of northwest China using multivariate statistical techniques and Bayesian mixing models. Journal of Cleaner Production, 379 (2), 134672.
31. Maher, B.A., Mutch, T.J., Cunningham, D., 2009. Magnetic and geochemical characteristics of Gobi Desert surface sediments: Implications for provenance of the Chinese Loess Plateau. Geology, 37(3), 279–282.
32. Marticorena, B., Bergametti, G., Gillette, D., 1997. Factors controlling threshold friction velocity in semiarid and arid areas of the United States. Journal of Geophysical Research, 102 (D19), 23277–23287.
33. Muhs, D. R., 2018. The geochemistry of loess: Asian and North American deposits compared. Journal of Asian Earth Sciences, 155, 81–115. https://doi.org/10.1016/j.jseaes.2017.10.032
34. Nie, J.S., Stevens, T., Rittner, M., Stockli, D., Garzanti, E., Limonta, M., Bird, A., Andò, S., Vermeesch, P., Saylor, J., Lu, H.Y., Breecher, D., Hu, X.F., Liu, S.P., Resentini, A., Vezzoil, G., Peng, W.B., Carter, A., Ji, S.C., Pan, B.T., 2015. Loess Plateau storage of Northeastern Tibetan plateau-derived Yellow River sediment. Nature Communication, 6 (1), 8511.
35. Prospero, J., 1999. Long-termmeasurements of the transport of African mineral dust to the southeastern United States: implications for regional air quality. Journal of Geophysical Research, 104 (D13), 15917–15927.
36. Pullen, A., Kapp, P., McCallister, A. T., McCallister, A. T., Chang, H., Gehrels, G. E., Garzione, C. N., Heermance, R. V., Ding, L., 2011. Qaidam Basin and northern Tibetan Plateau as dust sources for the Chinese Loess Plateau and paleoclimatic implications. Geology, 39(11), 1031–1034.
37. Rittner, M., Vermeesch, P., Carter, A., Bird, A. F., Stevens, T., Garzanti, E., Andò, S., GiovanniVezzoli, G., Dutt, R., Xu, Z.W., Lu, H.Y., 2016. The provenance of Taklamakan desert sand. Earth and Planetary Science Letters, 437, 127–13.
38. Shao, Y., Fink, A. H., Klose, M., 2010. Numerical simulation of a continental - scale Saharan dust event. Journal of Geophysical Research, 115, D13205.
39. Stevens, T., Carter, A., Watson, T.P., Vermeesch, P., Bird, A. F., Garzanti, E., Cottam, M.A., Sevastjanova, I., 2013. Genetic linkage between the Yellow River, the Mu Us desert and the Chinese Loess Plateau. Quaternary Science Reviews, 78(15), 355–368.
40. Stevens T., Palk, C., Carter, A., Lu, H.Y., Clift, P.D., 2010. Assessing the provenance of loess and desert sediments in northern China using U-Pb dating and morphology of detrital zircons. GSA Bulletin, 122 (7-8), 1331–1344.
41. Sun, J.M., 2002, Provenance of loess material and formation of loess deposits on the Chinese Loess Plateau. Earth and Planetary Science Letters, 203, 845–859.
42. Sun, J.M., Ding, Z.L., Xia, X.P., Sun, M., Windley, B.F., 2018. Detrital zircon evidence for the ternary sources of the Chinese Loess Plateau. Journal of Asian Earth Science, 155, 21–34.
43. Sun, Y.B., Yan, Y., Nie, J.S., Ki, G.J., Shi, Z., Qiang, H., Chang, h., An, Z.S., 2020. Source-to-sink fluctuations of Asian aeolian deposits since the late Oligocene. Earth-Science Reviews, 200, 102963.

44. Tan, Z.Y., Liu, YZ., Zhu, Q.Z., Shao, T.B., 2021. Impact of massive topography on the dust cycle surrounding the Tibetan Plateau. Atmospheric Environment, 264, 118703.
45. Tanaka, T., Chiba, M., 2006. A numerical study of the contributions of dust source regions to the global dust budget. Global and Planetary Change, 52, 88–104.
46. Vermeesch, P., 2013. Multi-sample comparison of detrital age distributions. Chemical Geology, 341, 140–146.
47. Webb, N.P., Okin, G.S., Brown, S., 2014. The effect of roughness elements on wind erosion: The importance of surface shear stress distribution. Journal of Geophysical Research Atmospheric, 119, 6066–6084.
48. Wu, G., Zhang, C., Gao, S., et al., 2009. Element composition of dust froma shallow Dunde ice core, Northern China. Global and Planetary Change, 67, 186–192.
49. Wyrwoll, K., Wei, J.H., Lin, Z.H., Shao, Y.P., He, F., 2016. Cold surges and dust events: Establishing the link between the East Asian Winter Monsoon and the Chinese loess record. Quaternary Science Reviews, 149,102–108.
50. Xuan, J., Liu, G.L., Du, K., 2000. Dust emission inventory in Northern China. Atmospheric Environment, 34, 4565–4570.
51. Zhang, Z.C., Bird, A., Zhang, C.X., Dong, Z.B., 2022a. Not all gravel deserts in northern China are sources of regionally deposited dust. Atmospheric Environment 273, 118984.
52. Zhang, Z.C., Dong, Z.B., Qian, G.Q., Jiang, C.W., 2016. Implications of surface properties for dust emission from gravel deserts (gobis) in the Hexi Corridor. Geoderma, 268, 69–77.
53. Zhang, Z.C., Dong, Z.B., Zhao, A.G., 2008. The effect of restored microbiotic crusts on erosion of soil from a desert area in China. Journal of Arid Environments, 7, 710–721.
54. Zhang, Z.C., Dong, Z.B., Zhao, A.G., 2011. The characteristics of aeolian sediment flux profiles in the southeastern Tengger Desert. Sedimentology, 58, 1884–1894.
55. Zhang, Z.C., Liang, A.M., Dong, Z.B., Zhang, Z.H., 2022b. Sand provenance in the Gurbantunggut Desert, northern China. Catena, 214, 106242.
56. Zhang, Z.C., Pan, K,J., Zhang, C.X., Liang, A.M., 2020. Geochemical characteristics and the provenance of aeolian material in the Hexi Corridor Desert, China. Catena 190, 104483.